I.A.U
Karaj branch

Journal of Applied Chemical Research
jacr.kiau.ac.ir

Journal of Applied Chemical Research, 19, 3, 57-76 (2025)

Preparation and Characterization of Flower- Shaped p-BiOI/n-ZnO for Photocatalytic Breakdown of Erythromycin Using Sunlight

Mohammad Hossein Ghorbani

Department of Chemistry, ST.C., Islamic Azad University, Tehran, Iran

(Received 13 Jul. 2025; Final revised received 24 Sep. 2025)

Abstract

This study presents the synthesis, structural analysis, and photocatalytic evaluation of a novel flower- shaped Zinc oxide, Bismuth Oxyiodide, and p-BiOI/n-ZnO heterojunction for the efficient degradation of erythromycin under sunlight. The unique morphology and band alignment of the heterojunction significantly enhance light absorption, charge separation, and pollutant breakdown efficiency.

These photocatalysts were characterized and tested for erythromycin degradation under sunlight. Using Design of Experiments, key parameters were evaluated: pH, time, catalyst mass, and erythromycin concentration. Optimal conditions achieved 99.14% degradation efficiency at pH 3, 102 minutes, 0.16 g catalyst, and 43.34 mg/L erythromycin. Isotherm studies revealed the best fit with the 4-parameter Fritz- Schlunder model. This research offers a promising solution for removing persistent antibiotics from aqueous environments, surpassing conventional treatment methods.

Keywords: Photocatalyst, BiOI, ZnO, Erythromycin, Sunlight degradation, p-n heterojunction.

[*] ***Corresponding author**: Mohammad Hossein Ghorbani, Department of Chemistry, ST.C., Islamic Azad University, Tehran, Iran, Email:MH_Ghorbani@iau.ac.ir.*

Introduction

The pervasive contamination of aquatic environments by pharmaceutical compounds, notably antibiotics, has emerged as a significant environmental and public health concern. Erythromycin, a widely prescribed macrolide antibiotic, is frequently detected in surface waters and wastewater effluents due to its extensive use and incomplete removal during conventional wastewater treatment processes [1,2]. The persistence of erythromycin in the environment is alarming, as it can induce antibiotic resistance and disrupt aquatic ecosystems [1,3]. Consequently, there is an urgent need for effective and sustainable methods to degrade such recalcitrant micropollutants.

Photocatalysis has garnered considerable attention as a promising advanced oxidation process for the degradation of persistent organic contaminants, including antibiotics, in water matrices [4,5]. This technique exploits semiconductor materials to harness solar or artificial light, generating reactive species capable of mineralizing organic pollutants. Among various semiconductors, titanium dioxide (TiO_2) has been extensively studied; however, its limited absorption in the visible spectrum and rapid recombination of photogenerated electron-hole pairs constrain its practical efficiency [4,6]. To overcome these limitations, the development of heterojunction photocatalysts composites that combine p-type and n-type semiconductors has shown great potential. Such heterojunctions enhance charge separation, extend light absorption into the visible region, and improve photocatalytic activity [7,8].

Bismuth oxyiodide (BiOI), a p-type semiconductor with a narrow bandgap, exhibits strong visible-light absorption and chemical stability, making it a promising candidate for photocatalytic applications [9,10]. Zinc oxide (ZnO), an n-type semiconductor, is known for its high electron mobility and environmental compatibility, but it suffers from rapid charge carrier recombination and limited visible-light response [11]. The construction of p-BiOI/n-ZnO heterojunctions can synergistically address these drawbacks, facilitating efficient charge separation and enhancing photocatalytic performance under solar irradiation [8-12]. Recent studies have demonstrated that the morphology of photocatalysts plays a crucial role in their activity; flower-shaped structures, in particular, offer increased surface area and more active sites, further boosting photocatalytic efficiency [9-13].

The application of sunlight-driven photocatalysis for antibiotic degradation is particularly attractive due to its sustainability and cost-effectiveness. Solar-light-activated photocatalysts have been shown to effectively degrade various antibiotics and reduce the abundance of antibiotic resistance genes in treated wastewater [14]. Despite these advances, the photocatalytic breakdown of erythromycin using flower-shaped p-BiOI/n-ZnO composites under sunlight remains underexplored.

This study aims to address this gap by focusing on the preparation and characterization of flower-shaped p-BiOI/n-ZnO heterojunctions and evaluating their efficacy in the photocatalytic degradation of erythromycin under sunlight. By leveraging the synergistic effects of the heterojunction structure and the unique morphological advantages, this research seeks to contribute to the development of efficient, solar-driven solutions for the remediation of antibiotic pollution in aquatic environments.

This approach has to eliminate all types of pollution and its applications include groundwater treatment, sludge degradation of industrial effluents and removal of volatile organic pollutants [15-20]. ZnO is a n-type semiconductor with a band gap has ranged from 3.10 eV to 3.37 eV. ZnO is one of the richest nanostructures in terms of morphological and application diversity. This diversity in morphology gives rise to unique features and applications in it. This material has spherical,

sheet, tube, rod, flower- like and star morphologies [21, 22]. ZnO is a metal oxide widely used in various industries due to its biocompatibility and safety including sunscreens, electrodes and biosensors, photocatalysis, and solar cells. ZnO also has moisturizing, antibiotic and deodorant properties. ZnO is widely used due to its semiconductor, wide band gap, high thermal resistance, pyroelectric and piezoelectric properties in addition to medical applications in other industries including water and wastewater treatment, optics, electronics, rubber, plastic, ceramics, glass, wood, cement, paint and glue [23].

Experimental

Materials and Methods

Zinc Acetate Dihydrate (Zn $(CH_3COO)_2$. $2H_2O$ 98%), Ammonia (NH_3 25%), Nickel Chloride ($NiCl_2$), Sodium oxalate ($Na_2C_2O_4$), Ethylene Glycol were purchased from Sigma- Aldrich Company. Erythromycin ($C_{37}H_{67}NO_{13}$ 20%) was prepared by Rooyan Darou Company. The chemical structure of erythromycin is demonstrated in Figure 1.

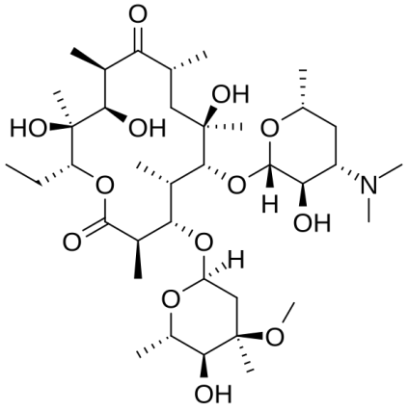

Figure 1. Configuration of erythromycin molecule.

Synthesis of BiOI particles

All chemicals used were of analytical grade, including bismuth nitrate pentahydrate ($Bi(NO_3)_3.\ 5H_2O$), potassium iodide (KI), zinc nitrate, sodium hydroxide, ethanol, and deionized water.

Synthesis of Flower- Shaped BiOI Particles

BiOI particles were synthesized using a solvothermal method. First, 2 mmol of $Bi(NO_3)_3.\ 5H_2O$ was dissolved in a mixture of 20 mL ethanol and 20 mL deionized water under magnetic stirring to form a clear solution. Separately, 2 mmol of KI was dissolved in 20 mL of deionized water. The KI solution was then added dropwise to the bismuth nitrate solution under continuous stirring, resulting in the formation of a reddish precipitate. The resulting suspension was transferred into a Teflon-lined stainless steel autoclave and heated at 160°C for 12 hours. After naturally cooling to room temperature, the precipitate was collected by centrifugation, washed multiple times with deionized water and ethanol, and dried at 60°C in an oven to obtain flower- like BiOI particles.

Synthesis of p-BiOI/n-ZnO Composite

ZnO nanoparticles were prepared using a precipitation method. The BiOI/ZnO composite was formed by dispersing BiOI into a ZnO precursor solution followed by annealing at 350°C.

Photocatalytic Degradation

The photocatalytic degradation of erythromycin (25 mg/L) was evaluated under sunlight using flower-shaped BiOI/ZnO composites at neutral pH (pH 7). The total catalyst mass was fixed at 0.1 g, with the BiOI content varied between 1 and 7 wt%. After 120 minutes of irradiation, the reaction mixtures were centrifuged at 4,500 rpm for 35 minutes to separate the catalyst. The residual concentration of erythromycin was determined by measuring the absorbance at 315 nm using UV–visible spectroscopy.

$$\text{Efficiency} = \frac{(A_0 - A_t)}{A_0} \times 100 \qquad (1)$$

Where A_0 is the initial absorption of erythromycin and at is its final absorption on the degradation.

DOE

In this study, RSM was used to model the degradation process. RSM is a powerful tool for statistical modeling that performs the least number of experimental experiments according to the experimental design. RSM itself has different types and this statistical method can be used in

different ways. Two common methods of central composite design (CCD) and Box–Behnken design (BBD) are RSM. One of the most common methods used to optimize various factors is the use of a CCD. This design is an alternative and suitable method for factorial design. The advantage of using a CCD over a factorial design is the possibility of extracting more information from the analysis of this design and the smaller number of experiments and iterations required to perform the experiment, which makes the implementation of this design easier.

The main regression equation to predict the effect of factors on the response is defined as follows:

$$Y = \beta_0 + \sum_{j=1}^{k} \beta_j X_j + \sum_{j=1}^{k} \beta_j X_j^2 + \sum_i \sum_{<j=2}^{k} \beta_j X_i X_j + e_i \qquad (2)$$

50 mL of erythromycin with different concentrations of 10-80 (mg/L) were prepared at pH 2-9 and with different mass of catalyst of 0.02-

0.2 (g) flower- like p-BiOI/n-ZnO (5%) was exposed to sunlight for 10-120 (min) Table 1. Also, under optimal conditions, the experiment was performed in the dark without sunlight.

Table 1. Independent variables and the levels in the experimental.

Independent variables	Coded Symbols	Levels
pH	X_1	2, 3, 5, 7, 9
Time (min)	X_2	10, 35,60, 100, 120
Mass of Catalyst (g)	X_3	0.02, 0.08, 0.10, 0.16, 0.2
Concentration of Erythromycin (mg/L)	X_4	10, 30, 45, 65, 80

Isotherm Studies

A solution of erythromycin with various concentrations ranging from 20 to 120 mg/L was prepared in a volume of 50 mL at a pH of 3. Afterwards, 0.16 g of a flower- like p-BiOI/n-ZnO (5%) photocatalyst was added, and the mixture was subjected to sunlight for 110 minutes. The study examined the photocatalytic degradation of erythromycin using the p-BiOI/n-ZnO (5%) photocatalyst under solar light, applying isothermal equations of 2, 3, and 4 parameters, while evaluating three types of errors for optimization. The resulting isotherms and calculated errors are presented in Tables 2 and 3, respectively.

Table 2. Lists of Adsorption Isotherms Models.

No. of Parameters	Isotherm	Nonlinear Form
2	Langmuir	$q_e = \frac{q_m \times b \times C_e}{1 + b \times C_e}$
	Freundlich	$q_e = K_f \times C_e^{\frac{1}{n}}$
	Tempkin	$q_e = B_T \times \ln(A_T \times C_e)$
3	Redlich- Peterson	$q_e = \frac{K_R \times C_e}{1 + a_R \times C_e^g}$
	Khan	$q_e = \frac{q_s \times b_K \times C_e}{(1 + b_K \times C_e)^{2K}}$
	Radke- Prausnitz	$q_e = \frac{a_{RP} \times r_{RP} \times C_e}{1 + r_{RP} \times C_e^{B_{RP}}}$
4	Fritz- Schlunder	$q_e = \frac{C \times C_e^{\alpha_{FS}}}{1 + D \times C_e^{\beta_{FS}}}$

Table 3. Explanation of Different Error Functions.

Error Functions	Abbriviation	Definition/Expression
Hybrid Fractional Error Function	Hybrid	$\frac{1}{n} = \sum_{i=1}^{n} \left[\frac{(q_{exp} - q_{cal}^2)}{q_{exp}} \right]_i$
Marquardt's Percent Standard Deviation	MPSD	$\frac{1}{n} = \sum_{i=1}^{n} \left[\frac{(q_{e,exp} - q_{e,cal})}{q_{e,exp}} \right]_i^2$
Average Relative Error	ARE	$\frac{1}{n} = \sum_{i=1}^{n} \left\| \frac{(q_{e,exp} - q_{e,cal})}{q_{e,exp}} \right\|_i$

Using Equation (3), the values of q_e were derived and graphically represented against C_e.

$$q_e = \frac{(C_o - C_e) \cdot V}{W} \qquad (3)$$

Here, q_e is the mass of pollutant adsorbed per unit mass of catalyst, C_0 and C_e are the initial and final concentrations of erythromycin, respectively. V is the volume of erythromycin solution (L) and W is the mass of the catalyst (g).

Results and discussion

The synthesis and analysis of ZnO flower- like, BiOI, and p-BiOI/n-ZnO flower- like catalysts were conducted using XRD technique. Figure 2 illustrates the XRD analysis results for the ZnO flower-like catalyst.

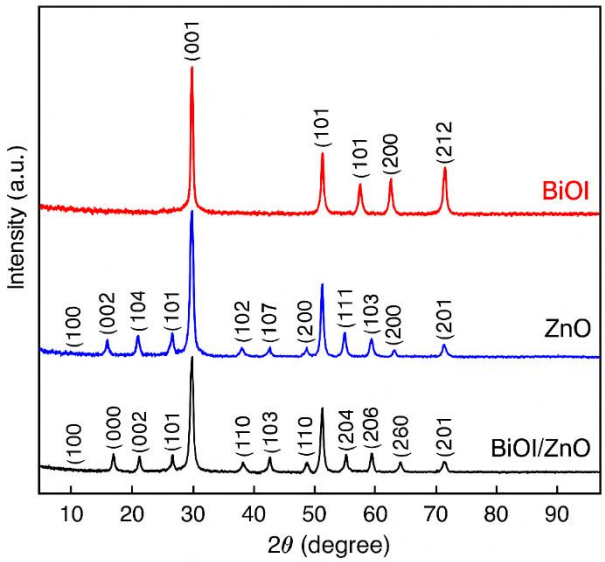

Figure 2. XRD pattern of BiOI, ZnO and BiOI/ZnO.

The XRD pattern for the ZnO flower- like structure shows peaks at 2θ values of 31.7, 34.4, 36.2, 47.5, 56.6, 62.9, 66.4, and 68.0, which correspond to the crystal planes (100), (002), (101), (102), (110), (103), (200), and (112) respectively, these match well with JCPDS card No. 36-1451. The XRD pattern for BiOI displays peaks at 2θ of 29.6, 31.6, 37.6, 39.4, 45.3, 55.2 and 61. 7, which are linked to the Miller indices (102), (110), (111), (200), (212), (213) and (220) respectively, suggesting a cubic phase (JCPDS card No. 10-0445). In the XRD Pattern of p-BiOI/n-ZnO flower-like structure, the diffraction peaks overlap may occur near ~31.7° (ZnO (100)) and ~31.6° (BiOI (110)). Based on Equation (4), the average particle size was calculated utilizing the Debye–Scherrer method:

$$B = \frac{K \cdot \lambda}{L \cdot \cos\theta} \qquad (4)$$

The average particle sizes determined using the Debye– Scherrer method were approximately 76 nm for ZnO, 24 nm for BiOI, and 92 nm for the flower- like p-BiOI/n-ZnO composite. The vibrational characteristics of the ZnO, BiOI, and flower- like p-BiOI/n-ZnO catalysts were analyzed through FT-IR spectroscopy. In the FT-IR spectrum of ZnO, a band at 430–550 cm^{-1} is indicative of the Zn–O stretching vibrations typical for ZnO. The peak at 1650 cm^{-1} corresponds to the H–O–H bending vibrations from physically adsorbed water molecules. Peaks at 1045 cm^{-1} are attributed asymmetric stretching vibration of Bi–I bond in BiOI and Broad peak ~3450 cm^{-1} is for O–H stretching vibrations due to surface hydroxyl groups or adsorbed moisture. For BiOI's FT-IR spectrum, peaks at ~500 cm^{-1} are assigned to the Bi–O stretching vibrations characteristic of BiOI structure. The Bi–I bond vibration around 1045 cm^{-1} is distinctive for BiOI. In the FT-IR spectrum of p-BiOI/n-ZnO, the peak observed at 531.45 cm^{-1} is related to Bi-O-I, while the peak at 548.43 cm^{-1} corresponds to the Zn-O bond. The peaks at 1628.78 and 3380.78 cm^{-1} are associated with H-O-H and O-H stretching, respectively (Figure 3). ZnO, BiOI, and the flower-like p-BiOI/n-ZnO were examined using FE-SEM (Figure 4). The FE-SEM results reveal that ZnO and BiOI exhibit flower- like and spherical morphologies, respectively, both at the nanoscale. Moreover, the findings indicate that BiOI particles are well distributed on the ZnO flower. The Xmap technique analyzes specific sample areas point-by-point, whereby EDS analysis is performed on numerous points in an assigned area, and the findings are presented as a series of colored dots, each representing a different element. In the p-BiOI/n-ZnO map images, the presence of Zn, Bi, and O is indicated by green, red, and blue dots, respectively. According to the EDS results, the amounts of BiOI (24.3%) and ZnO (75.7 %), in p-BiOI/n-ZnO confirm the high purity of the hybrid, as no other elements were detected in the sample (Figure 5).

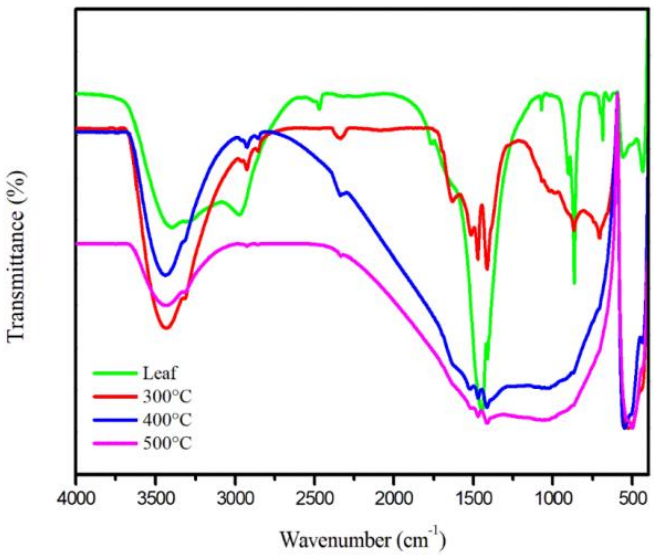

Figure 3. FT-IR spectrum of BiOI, ZnO and BiOI/ZnO.

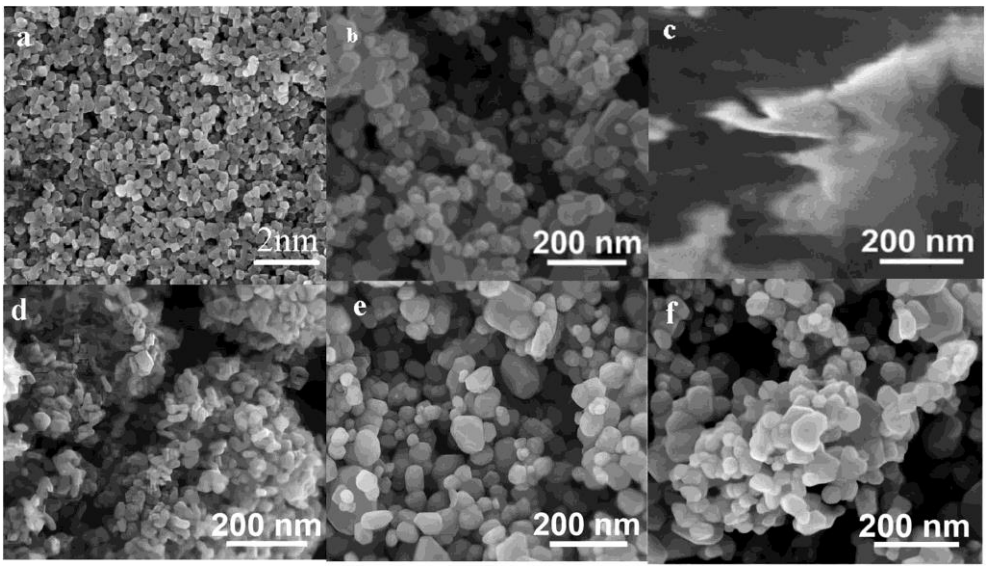

Figure 4. FE-SEM images of a,b) BiOI, c,d) ZnO e,f) BiOI/ZnO.

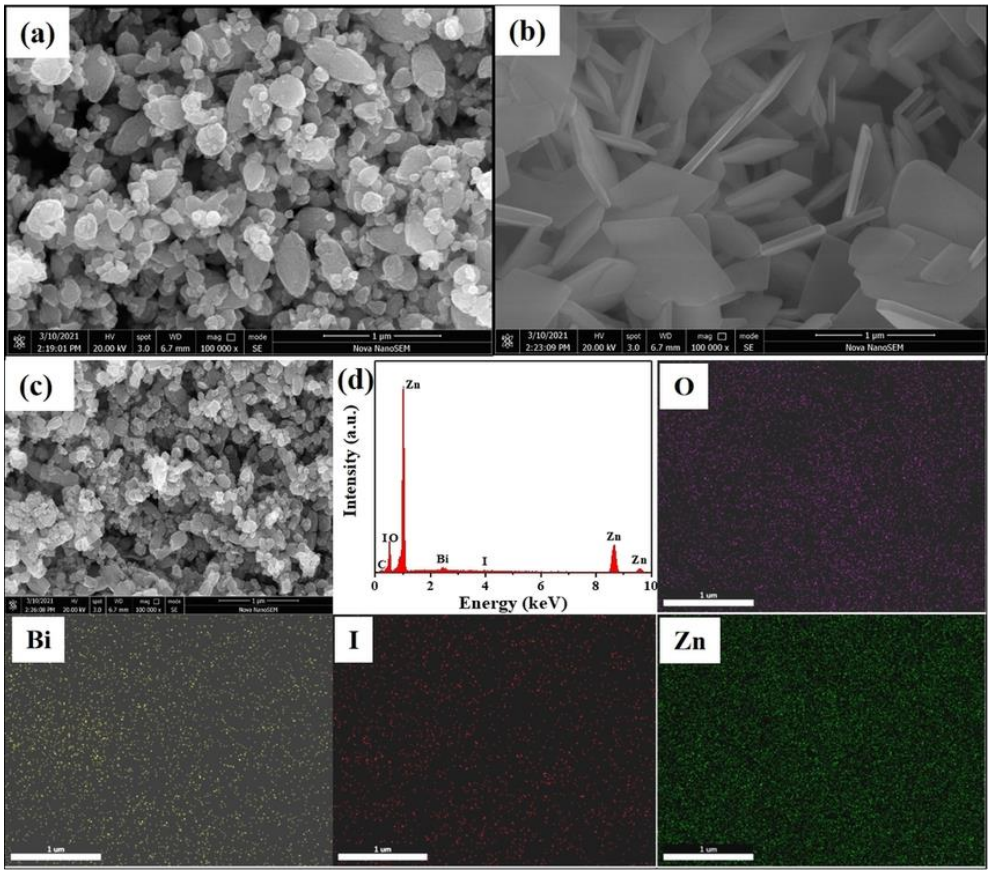

Figure 5. Map images of a) Zn, b) Bi, c) O, d) combine, e) EDS pattern of BiOI/ZnO and f) FE-SEM of BiOI/ZnO.

The BET method for measuring specific surface area is a physical analysis technique used to assess the specific surface area and porosity of materials. This approach, which relies on analyzing the adsorption and desorption of gases like nitrogen, is quick and relatively cost-effective; it enables statistical estimation of surface size, average particle size, porosity, shape, and size of the materials obtained. The findings for BiOI, ZnO, and p-BiOI/n-ZnO are presented in Figure 6 and Table 4.

Table 4. Results of BET/BJH Analysis for Various Catalysts.

Catalyst	a_s, BET ($m^2\ g^{-1}$)	Total Pure Volume ($cm^3\ g^{-1}$)	Mean Pure Diameter (nm)
ZnO	2.84	0.031	37.83
BiOI	76.55	0.268	14.85
BiOI/ZnO	5.47	0.036	33.62

According to these findings, the synthesized catalysts exhibit isotherm type IV characteristics. By incorporating BiOI onto ZnO, there is an increase in surface area, pore volume, and mean pore size.

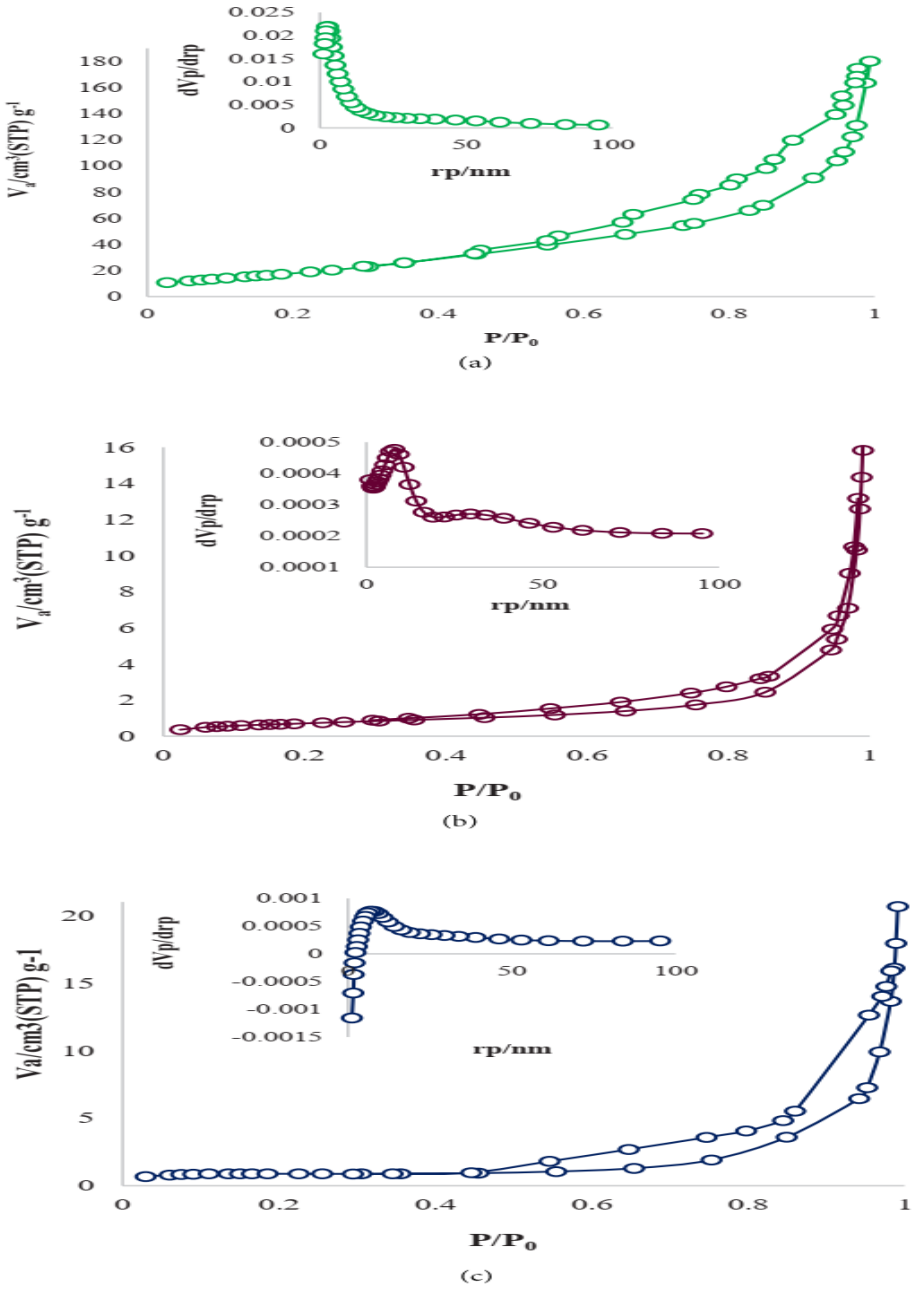

Figure 6. N_2 adsorption- desorption isotherms of a) BiOI, b) ZnO, and c) BiOI/ZnO.

Various methods exist for determining the optical band gap energy of semiconductor nanostructures, with the Tauc equation being one of the most widely used.

$$(\alpha \cdot h \cdot \nu)^{\frac{1}{n}} = A \cdot (h \cdot \nu - E_g) \qquad (5)$$

In this research, DRS and the Tauc diagram were employed to examine the transfer processes and ascertain the band gap energy of the synthesized photocatalysts. The findings revealed that the band gaps for ZnO, BiOI, and flower- like p-BiOI/n-ZnO were measured at 3.5 eV, 1.6 eV, and 2.7 eV, respectively (Figure 7).

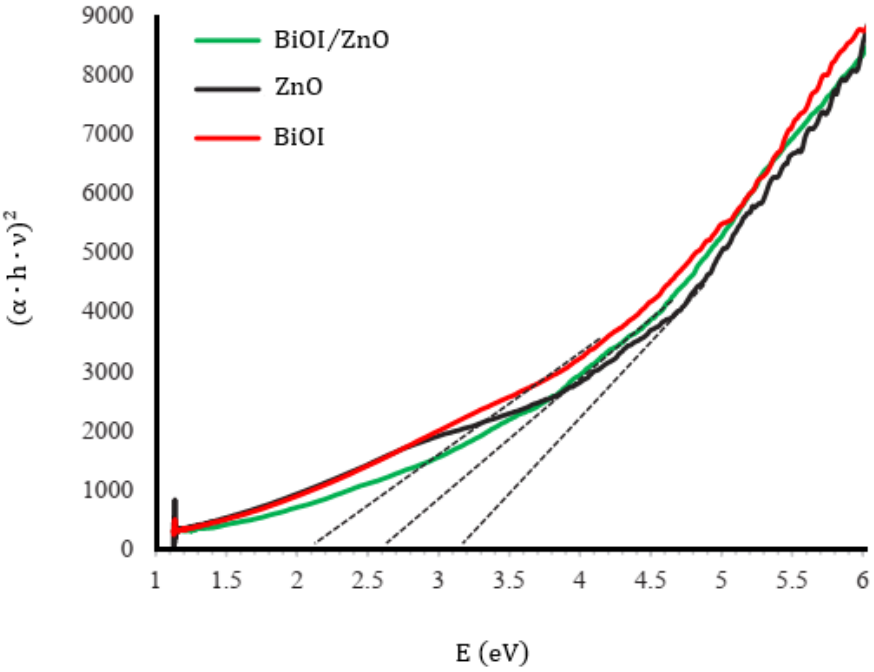

Figure 7. Band gap energies of BiOI, ZnO, BiOI/ZnO.

Effect of loaded BiOI (%)

The proportion of metal oxides significantly influences the effectiveness of the photocatalyst. In this research, to determine the optimal weight proportion of BiOI on ZnO support, BiOI samples with weight percentages of 1, 2, 5, and 7 were prepared and utilized for photocatalytic degradation. The findings indicate that as the weight percentage of BiOI rises from 1 to 5 wt%, the degradation efficiency improved from 75.00% to 99.99%. However, when the BiOI percentage increased from 5 to 7 wt%, the photocatalytic degradation efficiency declined from 99.99% to 60.00% (Figure 8). This decrease in efficiency occurs because the rise in BiOI from 5 to 7 wt% fills the pores of the

ZnO photocatalyst, thereby reducing light penetration into the catalyst's surface and resulting in diminished effectiveness.

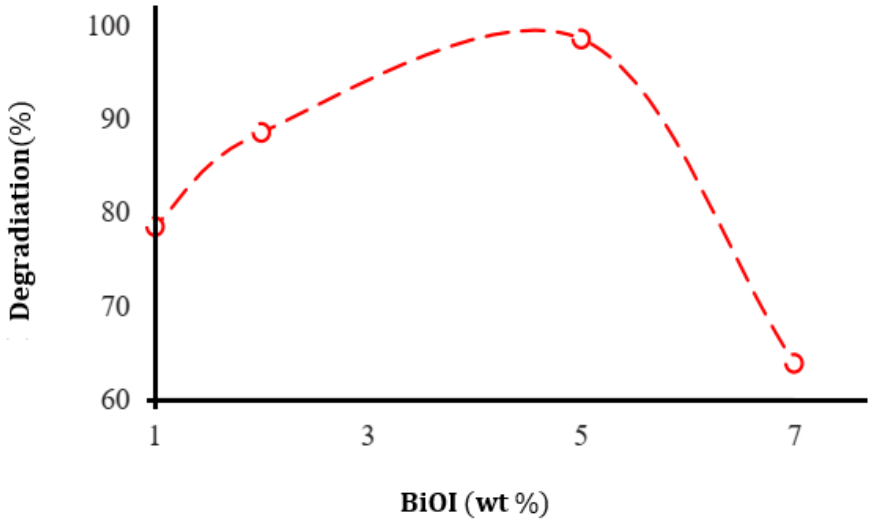

Figure 8. Effect of weight percentage of loaded BiOI.

Statistical Analysis

The outcomes of the photocatalytic breakdown of erythromycin utilizing the CCD method are illustrated in Table 5. A crucial aspect of the statistical evaluation of data is whether it follows a normal distribution, with the findings of this research illustrated in Fig. 9. Statistical analysis was conducted using an F-test and ANOVA to assess the variance in the quadratic model of the response surface, with the findings presented in Table 6.

The ANOVA results verify the validity of this quadratic model. The F parameter reflects how much the data deviates from the average value; generally, a successful model exhibiting predictive capability will have a notably high F-value, and P-values under 0.05 are indicative of a favorable model. For this model, the F-value is 43.84, demonstrating that the model holds significant relevance. Additionally, the R-Squared value for this model is 0.9843, consistent with an Adj R-Squared value of 0.9648, which reflects the model's accuracy.

Fig. 10 displays the disturbance diagram related to the photocatalytic degradation of erythromycin. Based on the results obtained, it can be concluded that the pH parameter (referred to as parameter A) exerts the most substantial influence on the photocatalytic degradation of erythromycin.

Effect of pH and time on erythromycin degradation efficiency

The starting pH level of the solution is a crucial factor in photocatalytic processes. To find the optimal pH, solutions with varying pH levels were created. The findings show that the degradation and oxidation percentages of erythromycin are influenced by the environmental pH. The results

indicate that as the pH decreases, the effectiveness of photocatalytic degradation improves since lower pH levels enhance the direct reduction via conduction band electrons, which significantly aids in the breakdown of erythromycin, thereby reducing the gap in its degradation. Additionally, erythromycin has a pKa of 8.9. The duration of degradation is a key factor in the breakdown of erythromycin. Longer degradation times result in increased energy consumption and higher refining expenses. Therefore, fine-tuning the process duration can reduce operational costs.

Table 5. The CCD for the 4 Independent Variables.

STD	Run	pH	Time (min)	Mass of Catalyst (g)	Concentration (mg/L)	Degradation (%)
7	1	3.0	102	0.16	30	99.14
5	2	3.0	35	0.16	30	78.50
12	3	3.0	102	0.05	65	98.45
25	4	5.5	65	0.10	80	67.74
30	5	5.5	65	0.10	45	64.27
10	6	3.0	35	0.07	65	96.13
18	7	2.0	65	0.10	45	93.34
5	8	7.0	35	0.16	30	82.17
10	9	7.0	35	0.07	65	53.26
15	10	7.0	102	0.16	65	62.43
20	11	5.5	35	0.10	45	75.64
30	12	5.5	65	0.10	45	64.32
12	13	7.0	102	0.07	65	53.78
15	14	7.0	35	0.16	65	69.56
1	15	3.0	35	0.07	30	78.32
30	16	5.5	65	0.10	45	64.91
20	17	9.0	65	0.10	45	33.38
25	18	5.5	65	0.10	45	64.22
28	19	5.5	65	0.10	45	67.86
14	20	3.0	35	0.16	65	88.72
25	21	5.5	65	0.12	45	65.31
22	22	5.5	65	0.12	30	94.14
5	23	7.0	102	0.07	30	82.03
20	24	5.5	65	0.03	45	79.64
3	25	7.0	35	0.07	30	66.47
15	26	3.0	102	0.16	65	90.02
25	27	5.5	65	0.20	45	98.83
3	28	3.0	102	0.07	30	99.12
20	29	5.5	120	0.12	45	96.37
10	30	7.0	102	0.16	30	87.52

The results of this study demonstrated that increasing reaction time correlates with improved efficiency. Figure 11 illustrates how pH and time influence erythromycin degradation efficiency through contour and 3D representations.

Table 6. ANNOVA for Analysis of Variance and Adequacy of the Quadratic Model.

Source	Sum of Squares	Degree of Freedom	Mean Square	F- Value	P- Value Prob > F
Model	8382.6	14	599.15	43.84	< 0.0001 Significant
A- pH	3864.29	1	3864.29	277.33	< 0.0001
B- Time	537.12	1	537.12	38.62	< 0.0001
C- Mass of Catalyst	261.53	1	261.53	19.44	0.0007
D- Concentration	613.87	1	613.87	45.69	< 0.0001
AB	75.38	1	75.44	6.14	0.0369
AC	252.51	1	586.62	18.21	0.0007
AD	633.57	1	15.93	0.37	< 0.0001
BC	24.38	1	752.19	18.42	0.2174
BD	273.41	1	239.75	5.72	0.0005
CD	7.77	1	388.29	9.31	0.4723
A2	0.99	1	1703.24	41.59	0.7973
B2	779.36	1	1792.03	42.98	< 0.0001
C2	521.11	1	347.14	8.61	< 0.0001
D2	210.35	1	728.27	18.54	< 0.0001
Residual	199.93	15	40.76		
Lack of Fit	9.01	10	58.97	9.82	
Pure Error	8592.31	5	5.84		0.0795

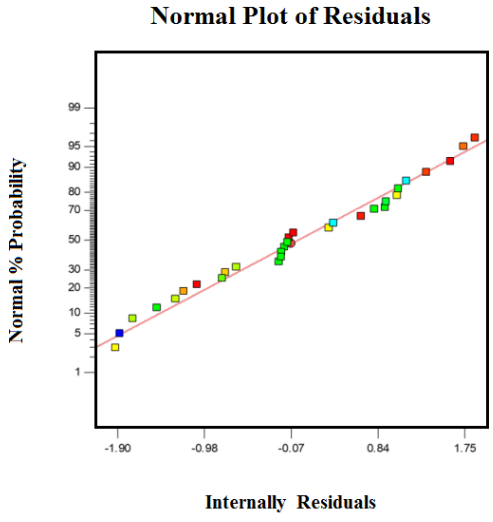

Figure 9. Normal probability plot of the residual for degradation of erythromycin.

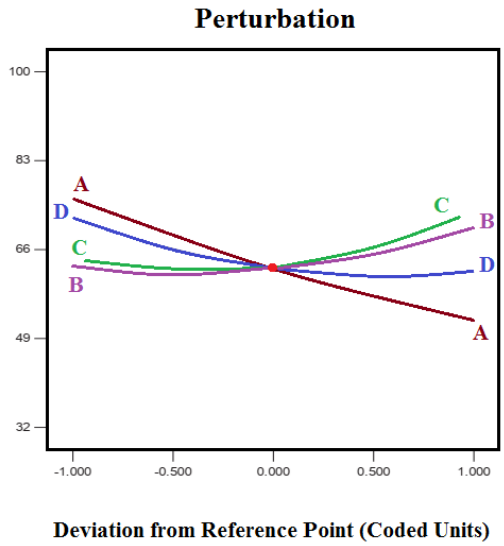

Figure 10. Perturbation plot for degradation of erythromycin.

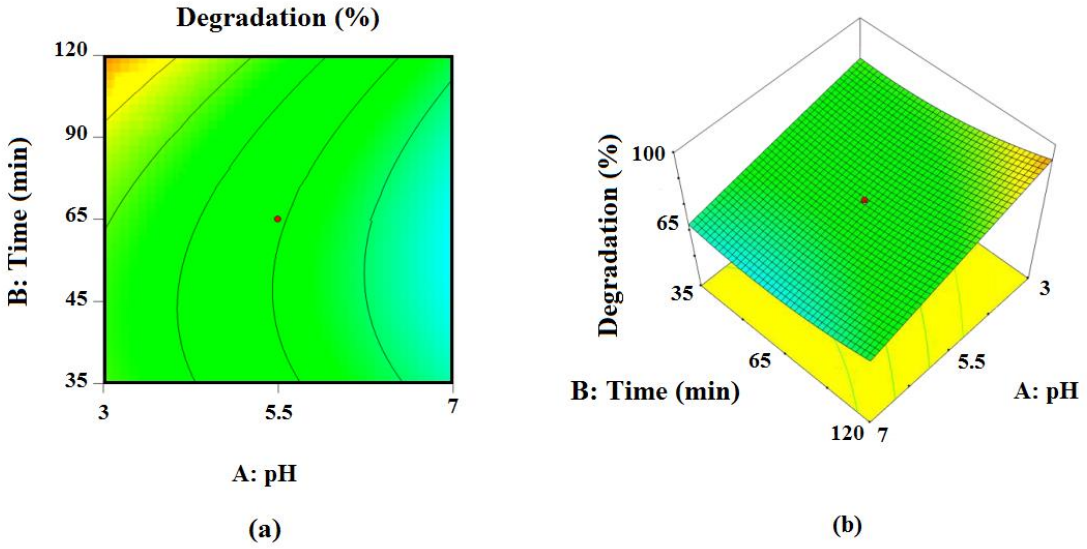

Figure 11. The Effect of pH and Time for Degradation of Erythromycin (a) Contour and (b) 3D Plot.

Effect of pH and photocatalyst mass on erythromycin degradation efficiency

The mass of the catalyst plays a crucial role in the degradation process. As the catalyst quantity rises, so does the efficiency; however, this improvement is beneficial only to a certain extent, beyond which the efficiency may decline. This occurs because an increase in catalyst mass enhances the number of active sites, leading to greater degradation efficiency. Conversely, a higher catalyst amount can also obstruct light penetration into the solution, as the increased presence of catalyst particles heightens the solution's turbidity, which negatively impacts erythromycin degradation efficiency, as illustrated in the contour and 3D plots (Figure 12).

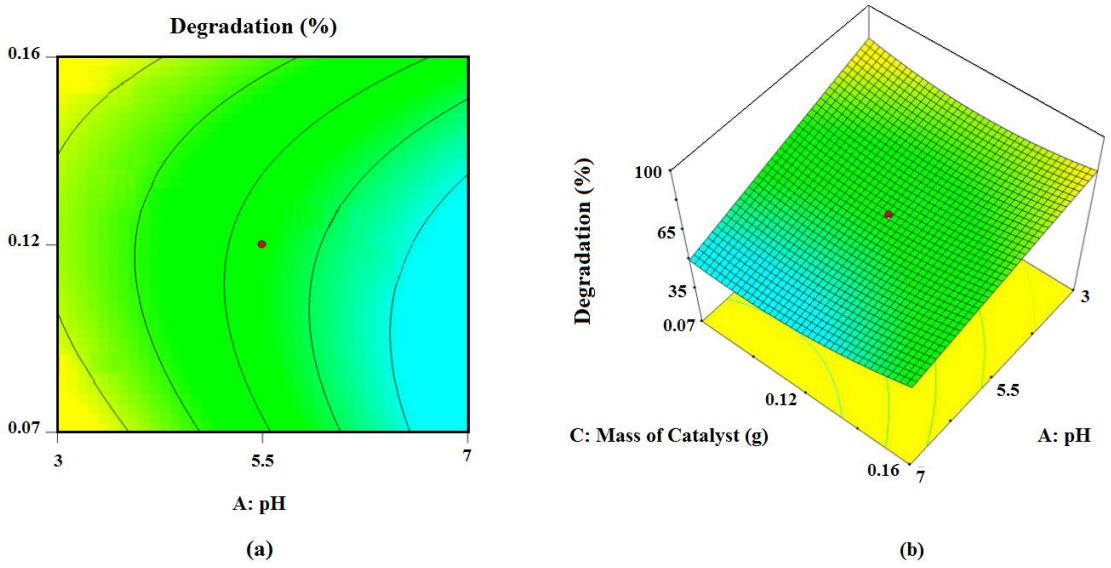

Figure 12. The Effect of pH and Mass of Catalyst for Degradation of Erythromycin (a) Contour and (b) 3D Plot.

Effect of pH and erythromycin concentration on erythromycin degradation efficiency

To assess the impact of erythromycin concentration, experiments were conducted within the range of 10-60 mg/L. The observed reduction in efficiency as concentration increases can be attributed to the fact that higher pollutant concentrations absorb emitted radiation, preventing it from reaching the photocatalyst surfaces. Figure 13 illustrates the influence of pH and erythromycin concentration on the degradation efficiency of erythromycin, presented as both contour and 3D plots.

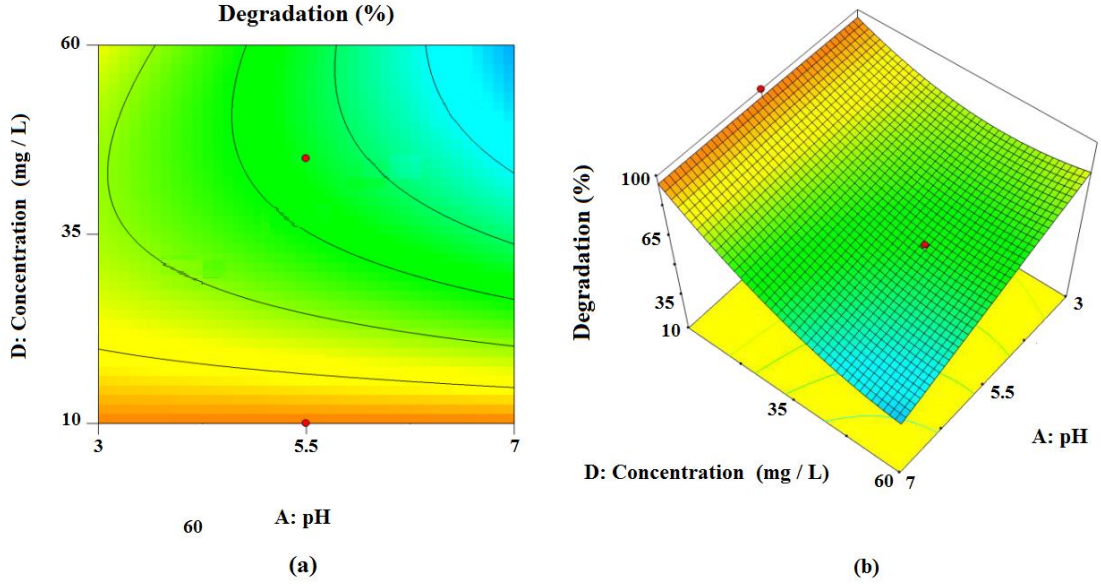

Figure 13. The Effect of pH and Mass of Concentration of Erythromycin for Degradation of Erythromycin (a) Contour and (b) 3D Plot.

Optimization

Ultimately, the analysis concluded that the ideal conditions for achieving the maximum degradation efficiency of erythromycin involve using a p-BiOI/n-ZnO (5%) photocatalyst with a mass of 0.16 grams, a reaction time of 102 minutes, an erythromycin concentration of 43.34 mg/L, and a pH of 3, resulting in a degradation rate of 99.14% (Figure 14).

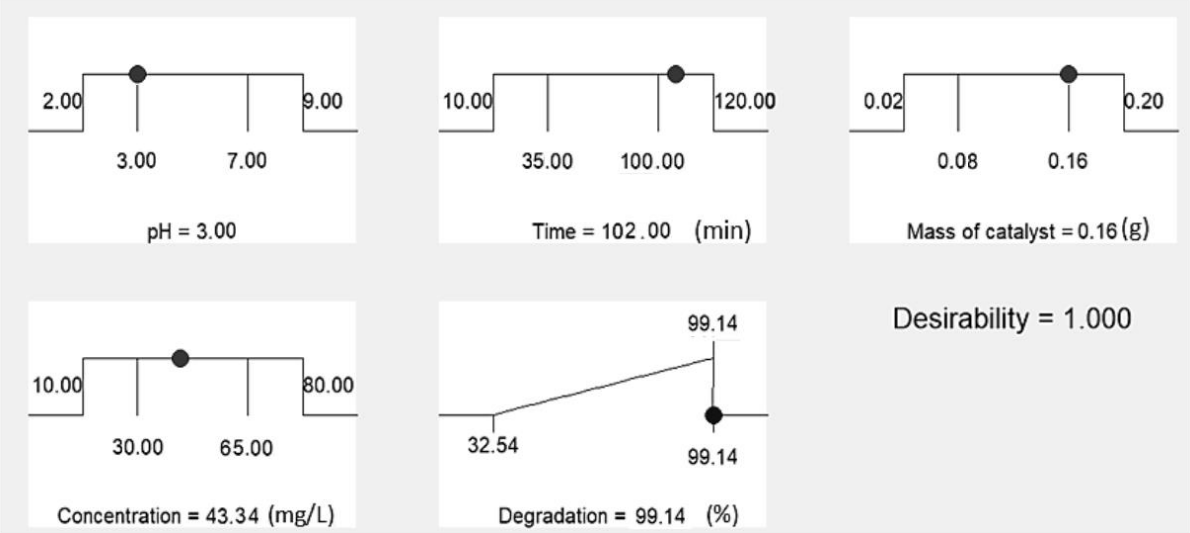

Figure 14. Graphs of the Optimum Condition for Degradation of Erythromycin.

Isothermal study

Revised experimental data were analyzed using 2, 3, and 4 parametric isotherms, and ultimately optimized through three error models (HYBRID, MPSD, and ARE). The outcomes of the isothermal analysis indicate that the Fritz-Schlunder isotherm provides the best fit, exhibiting the lowest error when compared to the experimental data for the photocatalytic degradation of p-BiOI/n-ZnO (Table 7).

Table 7. Isotherms and Error Functions for p-BiOI/n-ZnO Flower- Like (5%)

Isotherm	Isotherm Parameters	Error & R^2	Error Value & R^2
Langmuir		HYBRID	78.124
q_m	124.12	MPSD	20.013
b	0.15	ARE	0.8862
		R^2	0.6631
Freundlich		HYBRID	3.306
K_f	2.7136E-08	MPSD	0.1326
n	0.3241	ARE	0.1715
		R^2	0.9853
Tempkin		HYBRID	12.354
B_T	0.0017	MPSD	0.1489

A_T	231.24	ARE	0.3267
		R^2	0.9031
Redlich- Peterson		HYBRID	26.9687
K_R	0.1986	MPSD	0.6203
a_R	3.7136	ARE	0.5911
g	0.2415	R^2	0.8671
Khan		HYBRID	4.3125
q_s	0.00006	MPSD	0.0913
a_K	0.526	ARE	0.2764
b_K	2.4817	R^2	0.9812
Radke- Prausnitz		HYBRID	4.2365
a_{RP}	6.157	MPSD	0.0523
r_{RP}	2893	ARE	0.1634
B_{RP}	1.681	R^2	0.9819
Fritz- Schlunder		HYBRID	1.5186
C	5.2468	MPSD	0.0016
D	3.3127	ARE	0.0043
α_{FS}	0.0001	R^2	0.9989
β_{FS}	0.096		

Conclusion

In this research, ZnO and BiOI were deposited onto a flower- like structure of ZnO. The photocatalysts synthesized under sunlight were used to assess the degradation of the erythromycin antibiotic. Among the photocatalysts, flower- like p-BiOI/n-ZnO (5%) demonstrated the highest efficiency in degrading erythromycin. The degradation process of erythromycin by p-BiOI/n-ZnO (5%) was analyzed using Response Surface Methodology (RSM), and the results indicated that the software's statistical analysis was very precise, effectively expressing and analyzing the impact of various parameters. The optimal conditions for the photocatalytic degradation of erythromycin were identified as pH=3, a duration of 102 minutes, a photocatalyst mass of 0.16 grams, and an erythromycin concentration of 43.34 mg/L, achieving a degradation rate of 99.14%. Isotherm studies revealed that the Fritz- Schlunder isotherm provided the best fit to the experimental data for the photocatalytic degradation by p-BiOI/n-ZnO (5%), with minimal error.

References

1. Albornoz LL, Cortés JC, Vásquez MR, Orellana CA, Jara MA, Pérez JA. Removal of antibiotics in wastewater: Review. Chemosphere. 2021;263:128146.

2. Pazoki M, Ghasemzadeh R, Yavari M, Abdoli MA. Photocatalytic degradation of antibiotics using advanced materials. Nashrieh Shimi va Mohandesi Shimi Iran. 2018;37(4):101-110.

3. Felis E, Giebułtowicz J, Caban M, Wolska L, Stepnowski P, Nałęcz-Jawecki G. Occurrence and removal of pharmaceuticals in wastewater treatment plants. Sci Total Environ. 2022;812:152567.

4. Felis E, Giebułtowicz J, Caban M, Wolska L, Stepnowski P, Nałęcz-Jawecki G. Antibiotic resistance genes in treated wastewater. Sci Total Environ. 2022;830:154659.

5. Albornoz LL, Cortés JC, Vásquez MR, Orellana CA, Jara MA, Pérez JA. Removal of antibiotics in wastewater: Review. Chemosphere. 2021;263:128146.

6. Sillanpää M. Recent advances in photocatalysts for water treatment. Catalysts. 2021;11(1):55.

7. Zhang J, Wang Y, Li Q, Zhang L, Li X. BiOI flower-like microspheres: Synthesis and photocatalytic properties. RSC Adv. 2014;4(56):29523-29531.

8. Zhang M, Qin J, Yu P, Zhang B. Facile synthesis of a ZnO–BiOI p–n nano-heterojunction with excellent visible-light photocatalytic activity. Beilstein J Nanotechnol. 2018;9:72–83.

9. Zhang Y, Wang L, Li H, Chen J, Liu X. BiOI flower-like microspheres: Synthesis and photocatalytic properties. RSC Adv. 2014;4(56):29523-29531.

10. Kumar D, Singh R, Upadhyay VV, Raturi A, Saraswat M, Khan AK, Mohan C. Nanotechnology for environmental remediation. Front Nanotechnol. 2024;5:123.

11. Priyadarshini MC, Saranraj Iyyanar, Kuppusamy Kanagaraj, Priya SD, Yashwant Singh Bisht, Rohit Kumar. The nano frontier: emerging technologies for environmental remediation and sustainable energy. E3S Web Conf. 2024;588:01016.

12. Sharma G, Kumar A, Devi K, Sharma S, Naushad M, Ghfar AA, Ahamad T, Stadler FJ. Guar gum-crosslinked-Soya lecithin nanohydrogel sheets as effective adsorbent for the removal of thiophanate methyl fungicide. Int J Biol Macromol. 2018;114:295-305.

13. Liu J, Li H, Du N, Song S, Hou W. Synthesis, characterization, and visible-light photocatalytic activity of BiOI hierarchical flower-like microspheres. *RSC Adv.* 2014;4(56).

14. Hernández F, Fabregat-Safont D, Campos-Mañas M, Quintana JB. Efficient validation strategies in environmental analytical chemistry: a focus on organic micropollutants in water samples. Annu Rev Anal Chem. 2023;16(1):401–428.

15. Fernandes A, Makoś P, Boczkaj G. Treatment of bitumen post oxidative effluents by sulfate radicals based advanced oxidation processes (S-AOPs) under alkaline pH conditions. Journal of Cleaner Production. 2018 Sep 10;195:374-84.

16. Fard NE, Fazaeli R, Yousefi M, Abdolmohammadi S. Morphology-controlled synthesis of CuO, CuO rod/MWW composite for advanced oxidation of indole and benzothiophene. ChemistrySelect. 2019 Sep 6;4(33):9529-39.

17. Elmi Fard N, Fazaeli R, Yousefi M, Abdolmohammadi S. Oxidation of carbazole by shape-controllable Cu2O on MWW catalysis. Applied Physics A. 2019 Sep;125(9):632.

18. Saadi R, Saadi Z, Fazaeli R, Fard NE. Monolayer and multilayer adsorption isotherm models for sorption from aqueous media. Korean Journal of Chemical Engineering. 2015 May;32(5):787-99.

19. Fard NE, Fazaeli R. A novel kinetic approach for photocatalytic degradation of azo dye with CdS and Ag/CdS nanoparticles fixed on a cement bed in a continuous-flow photoreactor. International Journal of Chemical Kinetics. 2016 Nov;48(11):691-701.

20. Fard NE, Fazaeli R. Experimental design study of RB 255 photocatalytic degradation under visible light using synthetic Ag/TiO_2 nanoparticles: optimization of experimental conditions. Iranian Journal of Catalysis. 2018;8(2).

21. Zhu L, Li Y, Zeng W. Hydrothermal synthesis of hierarchical flower-like ZnO nanostructure and its enhanced ethanol gas-sensing properties. Applied Surface Science. 2018 Jan 1;427:281-7.

22. Zhu L, Li Y, Zeng W. Enhanced ethanol sensing and mechanism of Cr-doped ZnO nanorods: Experimental and computational study. Ceramics International. 2017 Dec 1;43(17):14873-9.

Djurišić AB, Chen X, Leung YH, Ng AM. ZnO nanostructures: growth, properties and applications. Journal of Materials Chemistry. 2012;22(14):6526-35.